

A geometrical model of DAS fibre response

Kris Innanen

ABSTRACT

A geometrical model of the shape and response of a buried DAS fibre, which allows for both a helical wind and arbitrary curvature of the cable, is a tool for analysis and appraisal of DAS experiments. The model takes as input vectors describing the cable shape and (optionally) the parameters of the helix. As output, the model generates arc-length, fibre positioning, and tangent information, with (optionally) a gauge length imposed. Five example applications of the model are presented: (1) the fibre may be embedded in modelled 3D elastic wave field and its response computed; (2) the 3C vector wave is reconstructed along the fibre within defined reconstruction windows; (3) the six components of tensor strain are reconstructed similarly; (4) the $\cos \theta$ directionality rule for P-wave displacement is generalized to the arbitrarily curved fibre; and (5) the $\cos^2 \theta$ directionality rule for P-wave strain is similarly generalized.

INTRODUCTION

Our growing ambitions for detailed analysis of seismic amplitude and phase information — both in quantitative interpretation/AVO inversion and full waveform inversion — raises the bar for seismic instrumentation and acquisition. Broader bandwidths, denser sampling, higher repeatability and amplitude and phase fidelity, all provided cheaply, will all be needed to bring multi-parameter FWI to the reservoir. The up and coming acquisition technology referred to as Distributed Acoustic Sensing (DAS), in which a fibre optic cable, rather than a geophone, senses seismic motion, appears to have the potential to fulfill a good portion of this demand. The purpose of this paper is to come to grips with some of the powerful and/or limiting aspects of the technology, and create a mathematical and numerical model allowing the interplay of limit and potential to be explored.

In the past five or so years, DAS-seismic technology has received some careful scrutiny (an early discussion was presented by Mestayer et al., 2011). DAS was tested by Shell as a cost-effective means for measuring vertical seismic profiling (VSP) data (Mateeva et al., 2012), and their positive impressions were followed up with discussions of its likely merits for deep water 4D VSP monitoring (Mateeva et al., 2013) and quantitative details regarding the fibre response (Mateeva et al., 2014). Subsequent reports of deep water DAS monitoring suggest that driving the costs even lower is the main current challenge (Chalenski et al., 2016). No *entirely technical* aspect of DAS acquisition has yet been pointed to as blocking its widespread use, which is encouraging.

This is not to say there are no technical limitations. Daley et al. (2013) review some of the history of development of the optical technology (*opto-electronics*) which has enabled DAS, and report on several field tests of fibre in a walkaway VSP configuration as a means to monitor CO₂ injection and storage. Reduced sensitivity and signal-to-noise ratio of DAS relative to clamped geophones appears to have been the key limiting issue in these tests. In spite of these challenges, the use of DAS systems to carry out sensitive processing

tasks such as noise correlation and interferometry has gone forward (Ajo-Franklin et al., 2015). Vendors have weighed in also, validating with laboratory results that amplitude and phase responses from fibre correlate closely with the acoustic field illuminating the fibre (Parker et al., 2014). Spatial sampling is also limited. Although DAS sensing is sometimes referred to as “continuous” sensing (because all regions along the fibre respond to the seismic wave), it has what amounts to a spatial bandwidth. The light backscattered from regions experiencing seismic strain along the fibre strain is weak, and signal must be integrated over a finite length of the fibre in order to rise above the noise level. This characteristic interval is referred to as the *gauge length*, with 1m being the current state of the art. (Vendors presenting at this year’s EAGE DAS workshop made several references to new fibre materials with strong backscatter response, so we may see gauge lengths shorten in the coming years.)

In this paper we will be primarily concerned with analyzing a further technological limitation caused by the natural response of DAS systems to elastic wave motion (Mateeva et al., 2012, 2013, 2014) which is the strong directionality (i.e., angle-dependence) arising from the fibre’s sensitivity only to the component of longitudinal (or normal) strain parallel to the axis of the fibre. In words, this means that the fibre only responds to being stretched or squeezed in its long, or axial, dimension, i.e., the direction tangent to the fibre. When, for instance, a P-wave is incident broadside onto a fibre, and the strain caused by the wave is therefore at 90° to the fibre axis, almost no response is to be expected. A theoretical analysis of this and a model of the fibre’s elastic response is given by Kuvshinov (2016). This must be expected to have a significant negative effect on fibre when deployed in walkaway VSP, cross-well, and near offset surface reflection configurations. Mateeva et al. (2012) refer to this as the *broadside insensitivity* issue, and we will follow suit.

Alteration of the geometry of the fibre is a natural way of mitigating broadside insensitivity (Mateeva et al., 2014; Kuvshinov, 2016). If the shape of the fibre is altered from a straight line to form a curve, for instance by being twisted into a helix, it no longer “explores” with its tangent only one direction in the field- or laboratory-frame of reference, and so the special combination of tangent direction and strain direction leading to broadside insensitivity occurs less frequently along the fibre. This paper focuses on curvature in the fibre, and what possibilities expanding its use in DAS systems may have.

The main feature of the mathematical model of the fibre we are introducing is attention to geometry. By increasing the degree and kind of curvature the fibre in a DAS acquisition system experiences we increase the aspects of the propagating elastic wave that can be said to have been measured, but we simultaneously increase the complexity of the fibre response. Suppose a fibre arranged in a strongly curved shape (a helix wound around another helix, for instance) is illuminated by a vector elastic field, and suppose further that between 2310m and 2311m along the fibre we measure a strain which contributes unique information about the full (vector) elastic disturbance. This is good news, of course, but use of this unique information is not necessarily simple. What part of the vector exactly (in a 3C coordinate system defined on the surface of the Earth) is being sensed? Also, though we know it comes from a point 2310m along the *arc-length* of the fibre, if the arc-length traces out a helix within a helix, to what point in space does this arc-length correspond? These quantities can be kept track of and/or estimated, but only with a reasonably carefully-

designed geometrical model in hand. The main contribution in this paper is the formulation of such a model.

In the remainder of this introductory section we (1) give an overview of the geometrical model, including its basic input and output and the five applications we have so far developed for it, and then (2) we give a qualitative discussion of the physical basis for DAS, in particular distinguishing the range of types of optical scattering and highlighting the type in operation during DAS sensing. Following this the paper is divided up into two main sections. In the first of these two the geometrical model is set out, and in the second the model is applied. Demos of the Matlab codes implementing the model are provided also.

Geometrical DAS/fibre model overview

The inputs to the model are

1. A set of three vectors which describe the positioning in 3D space of the axis of the cable containing the fibre;
2. Parameters of the helix described by the fibre as it winds around the cable axis; and
3. Optical and response characteristics of the fibre (e.g., gauge length) and parameters of all estimation problems (e.g., 3C reconstruction window size, source location for directivity characterization).

The model begins by computing all of the secondary geometrical features of the fibre, which (now) can experience quite a complex degree of curvature. This includes

1. Arc-length s' along the cable axis;
2. A set of Cartesian unit vectors built around the tangent directions of the cable axis (one for each unit of arc-length along the cable) ;
3. Arc-length s along the fibre;
4. A set of three vectors which describe positioning of the fibre in 3D space;
5. A set of Cartesian unit vectors built around the tangent directions of the fibre (one for each unit of arc-length along the fibre);

Items (3.)-(5.) above are next averaged and re-sampled to reflect the gauge length as specified by the user in the input. Finally, the model is applied in each of several modes to characterize aspects of the response of the fibre. Currently there are four applications:

1. **The fibre is embedded in an input snapshot of a 3D elastic wave field, and the response of the fibre to the field is computed.** The wave field should be provided as three 3D arrays, each containing one component of the elastic displacement field. The fibre (with or without a gauge length imposed) is embedded in this field, and is assumed to be sensitive to the component of displacement in the direction tangent to the fibre at all points along its length. The output is a vector of components of tangential displacement of the same size as the vector of arc-lengths along the fibre.
2. **The 3C vector displacement field is reconstructed from a known fibre geometry and measurements of the elastic displacement tangent to the fibre at all points along its length.** This occurs over a reconstruction window which should be chosen to be (a) sufficiently large for the fibre within it to explore a significant range of

tangent directions, but (b) sufficiently small so that the displacement field may be assumed to be approximately constant within it. This application requires us to assume that from the tangential strain the tangential displacement can be estimated through some calibration.

3. **The 9C strain tensor field is reconstructed from a known fibre geometry and measurements of the longitudinal strain tangent to the fibre at all points along its length.** This requires no assumption about the calibration of strain component to displacement component, but it does require the fibre to explore sufficient directions within the reconstruction window to constrain six independent parameters instead of three.
4. **The broadside displacement curve for incident plane P-waves is generalized.** The phenomenon discussed by Mateeva et al. (2014) and Kuvshinov (2016) for straight and helical fibres is generalized to the case of a helix winding around an arbitrarily curved cable axis. The user-input source position and the fibre geometry are used to construct angles of incidence at each point along the fibre, and the P-wave displacement vector is projected onto the fibre tangents with these angles. The resulting curves, which can be inspected to quantify broadside directionality and sensitivity in any proposed experimental configuration, reduces to the familiar $\cos \theta$ rules given the special case of a straight fibre.
5. **The broadside strain curve for incident plane P-waves is generalized.** The phenomenon also discussed by Mateeva et al. (2014) and Kuvshinov (2016) for straight and helical fibres is generalized to the case of a helix winding around an arbitrarily curved cable axis. With the same inputs the P-wave strain tensor is projected onto the fibre tangents with these angles. The resulting curves, which can be inspected to quantify broadside directionality and sensitivity in any proposed experimental configuration, reduces to the familiar $\cos^2 \theta$ rules given the special case of a straight fibre.

Physical basis for DAS

Distributed Acoustic Sensing relies on the tendency for light to reflect from regions within an otherwise transparent medium which are experiencing some mechanical distortion. In this section we provide a qualitative discussion of the types of optical scattering in real media and their relation (or not) with fibre-optic sensing technology. Most of these phenomena are described quantitatively in the classic optics texts (e.g., Born and Wolf, 1999).

Rayleigh scattering

The interaction of light and matter is a very complicated process in general, particularly when light of high energy interacts with substances whose particulate components are large compared to the wavelength. A scale quantity is often introduced

$$x = \frac{2\pi r}{\lambda}, \quad (1)$$

whereby if the characteristic radius of the particles illuminated is r and the wavelength of the light is λ , the cases $x \ll 1$ and $x \gg 1$ are found to require different theoretical

treatment. Those of us with seismic backgrounds can intuitively see why: if the object is large, i.e., $x \gg 1$, the wave scattering from it is complex, usually with a new phase character different and more complex than that of the incident wave. If the object is small, i.e., $x \ll 1$, there is some directionality but much of the phase character of the incident wave is preserved. In optics when $x \gg 1$ the process is described in terms of *Mie* scattering; when $x \ll 1$ it is described in terms of *Rayleigh* scattering. Rayleigh scattering has the property that the re-radiated light has the same phase character as the incident light. However, the scattered light involves a strong ($\sim \lambda^{-4}$) wavelength dependence, with longer wavelengths tending to transmit un-impeded through a particulate medium and shorter wavelengths tending to scatter*.

As the energy of the light increases, its wavelength decreases, and the smaller the particles must be in order for scattering to be of Rayleigh type. Other factors begin to become important in such regimes also. Simple scattering of light occurs because particles of matter are polarized by the incoming electric field, meaning that positively and negatively charged components move relative to one another. Since all accelerating charges radiate, this motion induces light to propagate away from the particle. When energies are low, all of the incoming light either stays as it is or re-radiates in this way. Such scattering is referred to as *elastic*. When the energy of the incident light increases, the probability that internal degrees of freedom within the particle and its neighbours will be set in motion by it increases. If some of the incident energy excites motion which re-radiates differently and/or with lower energy, the scattering is referred to as *inelastic*. *Raman* scattering methods are used to describe such processes.

Other related optical scattering terms

Bragg scattering. These are optical scattering phenomena which occur when (1) the particles under illumination are in an orderly (e.g., crystalline) configuration, and (2) the wavelength of the incident light is on the order of the interval between particles. This process is not active in general in fibre-optic systems because glass is non-crystalline, that is its microscopic structure is not orderly.

Brillouin scattering. These are scattering phenomena which occur in a medium (e.g., glass) within which acoustic waves are simultaneously propagating; acoustic distortions affect the index of refraction of the medium which in turn affects the propagation of light. On a microscopic scale, because acoustic disturbances and the dielectric polarization phenomena which cause Rayleigh scattering both concern distortions of the particles and their constituents, the two can be conflated. However, the two processes cause quite different things to happen to backscattered light. Most notably, Brillouin scattering, because the interaction is with moving variations in the index of refraction, is subject to a Doppler shift and so the signal is dominated by a phase shift. This phase shift is the basis for temperature sensing fibre technology.

*So, no matter how mainstream DAS gets, it will always be blue sky research.

Single and multi-mode optical fibres

DAS fibre technology may be *single-mode* or *multi-mode*, by which the following is meant. The fibre acts as a wave guide. The propagating light travels along the fibre with a path that is not parallel to the axis of the fibre, and so it regularly impinges on the wall of the fibre. However, the angle between the path and the axis is sufficiently small that whenever this occurs the light undergoes total internal reflection, such that it nearly losslessly reverberates along the fibre. It does so with a characteristic velocity as measured along the fibre axis, which depends on the angle with which the light entered the fibre. Light which enters the fibre at one distinct angle and thereafter exhibits this characteristic reverberation and axial velocity is considered to constitute a *mode*. If one mode propagates in the fibre, the fibre is said to be *single-mode*; if more than one mode propagates in the fibre, the fibre is said to be *multi-mode*. Multi-mode fibres are larger to admit a wider range of angles of entry.

GEOMETRICAL MODEL OF DAS CABLE AND FIBRE

In this section we will describe the positioning of the cable/fibre system in a geological volume. This is critical so that the components of strain contributing to the fibre signal can be computed at any desired point along its length. Some standard results of differential geometry are required for which we use the text of Kreyszig (1991). The model is built up through geometrical considerations of the axis of the cable containing the fibre and the helical shape of the fibre within the cable, in the following order:

1. Cable geometry
 - (a) Cable axis position \mathbf{c}
 - (b) Arc-length s' along the cable axis
 - (c) Axial tangents
2. Fibre geometry
 - (a) Fibre position $\mathbf{f} = \mathbf{c} + \mathbf{h}$
 - (b) Arc-length s along the fibre
 - (c) Fibre tangents
3. Gauge length

1. Cable geometry

1a. Cable axis position

Let any point along a fibre (wound in a helix along a cable which itself may not be a straight line), be described with the position vector \mathbf{f} . Furthermore let \mathbf{f} have two parts. The first part, \mathbf{c} , is a vector pointing from the origin to the position along the central axis of the cable which is nearest to \mathbf{f} . The second part, \mathbf{h} , sits in the plane perpendicular

to the cable axis, and points from the cable axis to the actual fibre, which winds about the axis in a helix. At any point along the fibre we have

$$\mathbf{f} = \mathbf{c} + \mathbf{h}. \quad (2)$$

We will begin with \mathbf{c} , whose job it is to describe the shape of the cable as a curve embedded in a 3D volume. Its three components are parameterized by a single scalar variable, s' , which we will choose to represent *arc-length along the cable*. A point that is a distance s' along the centre of the cable then has position

$$\mathbf{c}(s') = \begin{bmatrix} c_1(s') \\ c_2(s') \\ c_3(s') \end{bmatrix}, \quad (3)$$

in terms of its components in the Cartesian system defined by the unit vectors $\{\hat{\mathbf{x}}_1, \hat{\mathbf{x}}_2, \hat{\mathbf{x}}_3\}$, which, for simplicity, we will write

$$\{\hat{\mathbf{1}}, \hat{\mathbf{2}}, \hat{\mathbf{3}}\}. \quad (4)$$

An example curve of this kind is illustrated in Figures 1a and b. We will generally associate $\{\hat{\mathbf{1}}, \hat{\mathbf{2}}, \hat{\mathbf{3}}\}$ with in-line, cross-line and depth directions respectively.

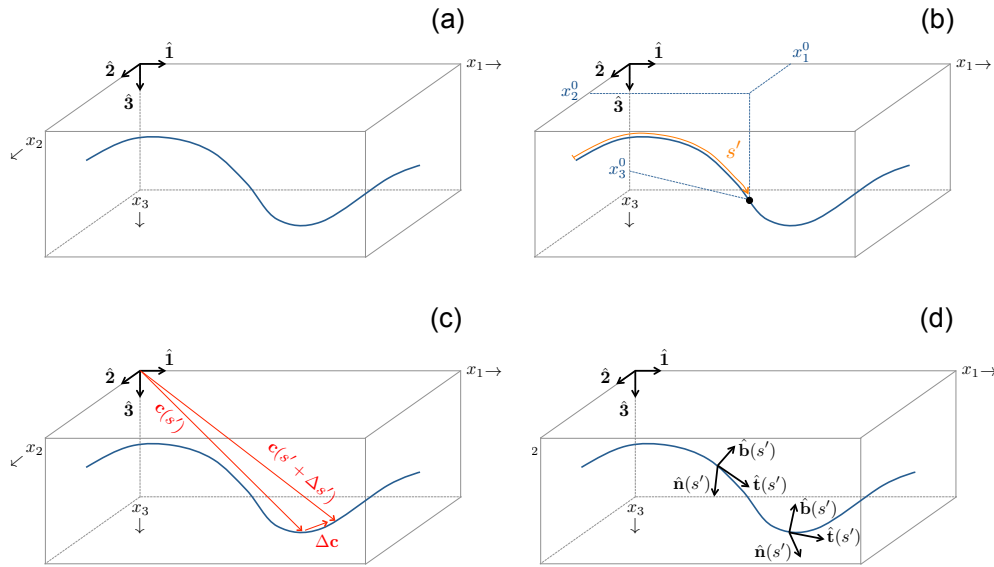


FIG. 1. (a) A curve $\mathbf{c}(s')$ embedded in a 3D medium is the starting point of a mathematical description of the axis of a buried DAS cable. (b) The curve is expressed by a vector that points to each position along the curve, moving from one point to the next as we change the scalar parameter s' . So to prescribe the curve we need to supply three functions of s , one for each component of the position vector. (c) The tangent to the curve $\hat{\mathbf{t}}(s')$ can be computed by taking the vector difference between two nearby points, and normalizing it by the arc-length between them; this becomes $\hat{\mathbf{t}}(s')$ in the limit. (d) Starting with the tangent direction, a Cartesian coordinate system can then be defined which characterizes the curve locally.

Especially for practical implementation of the model, it is convenient to include a second parameterization in which s' is eliminated in favour of one of the Cartesian coordinates, which thereafter acts as an independent variable. Choosing c_1 to be this coordinate,

and designating it as independent by renaming it x :

$$x = c_1, \quad (5)$$

we produce the alternative representation

$$\mathbf{c} = \begin{bmatrix} c_1(s') \\ c_2(s') \\ c_3(s') \end{bmatrix} = \begin{bmatrix} x \\ c_2(x) \\ c_3(x) \end{bmatrix}. \quad (6)$$

1b. Arc length s' along the cable axis

To keep track of the path length s' associated with a given point within this alternative parameterization, we make use of the formula:

$$s'(x) = \int_0^x dx' \left[\frac{d\mathbf{c}}{dx'} \cdot \frac{d\mathbf{c}}{dx'} \right]^{1/2} = \int_0^x dx' \left[1 + \left(\frac{dc_2}{dx'} \right)^2 + \left(\frac{dc_3}{dx'} \right)^2 \right]^{1/2}. \quad (7)$$

With either $c_2(x)$ and $c_3(x)$, or $c_1(s)$, $c_2(s)$ and $c_3(s)$ given, equation (6) alone or equations (6)-(7) together can be used to determine the positions in our Cartesian system of all points along the curve, and the arc-length along the curve at any point.

1c. Axial tangents

At any point along the curve $\mathbf{c}(s')$ we may calculate a new set of orthogonal directions, corresponding to the local character of the curve itself, generating a Cartesian coordinate system that changes as it follows the curve. This s -dependent system is defined in terms of the tangent to the curve, and two further orthogonal unit vectors occupying the plane normal to the tangent.

Consider two closely-spaced positions along a curve, $\mathbf{c}(s')$ and $\mathbf{c}(s' + \Delta s')$ as illustrated in Figure 1c. The direction of the vector difference between these positions, $\Delta\mathbf{c}$, will converge to that of the tangent as $\Delta s'$ vanishes. In fact, the unit tangent vector is defined as

$$\hat{\mathbf{t}}(s') = \frac{d\mathbf{c}}{ds'} = \lim_{\Delta s' \rightarrow 0} \frac{\mathbf{c}(s' + \Delta s') - \mathbf{c}(s')}{\Delta s'}. \quad (8)$$

If the tangent varies continuously along the curve (which we must assume to be true in order to describe a general deviated cable), that variation can be used to define two orthogonal unit vectors in the plane normal to the tangent. Any differential change in $\hat{\mathbf{t}}(s')$ with s' , since its length is always 1, must be perpendicular to $\hat{\mathbf{t}}(s')$ itself. Therefore one viable unit vector is $\hat{\mathbf{n}}(s')$, where

$$\hat{\mathbf{n}}(s') = \frac{\mathbf{n}(s')}{|\mathbf{n}(s')|}, \quad \mathbf{n}(s') = \frac{d\hat{\mathbf{t}}(s')}{ds'}. \quad (9)$$

This is referred to as the principal normal. Assuming sufficient curvature is present[†], the third unit vector, referred to as the binormal, can then be calculated as

$$\hat{\mathbf{b}}(s') = \hat{\mathbf{t}}(s') \times \hat{\mathbf{n}}(s'). \quad (10)$$

Now, as s' or x are varied, i.e., as we move back and forth along the deviated cable, we have a continuously changing Cartesian coordinate system oriented along the axis of the cable:

$$\left\{ \hat{\mathbf{t}}(s'), \hat{\mathbf{n}}(s'), \hat{\mathbf{b}}(s') \right\}, \quad \text{or} \quad \left\{ \hat{\mathbf{t}}(x), \hat{\mathbf{n}}(x), \hat{\mathbf{b}}(x) \right\}, \quad (11)$$

as illustrated in Figure 1d.

2. Geometry of the helical fibre

2a. Fibre position

A helix of radius r winding about the $x = x_1$ axis in the inline-crossline-depth Cartesian system can be expressed in the parameterized form

$$\mathbf{f}(t) = \begin{bmatrix} f_1(t) \\ f_2(t) \\ f_3(t) \end{bmatrix} = \begin{bmatrix} vt \\ r \cos t \\ r \sin t \end{bmatrix}. \quad (12)$$

If t were interpreted notionally as time, for instance, this helix could be understood as a circle of radius r being described in the (x_2, x_3) plane at a rate of $1/2\pi$ cycles per second, with the centre of that circle advancing along the $x = x_1$ axis at speed v . In a fibreoptic system the *lead angle*, rather than a rate quantity like v , is used to characterize the helix. To form this angle we compare (1) the *lead*, i.e., the distance l a particle moving along the helix travels in the axial (x) direction over the course of one complete rotation, against (2) the perimeter of the envelope of the helix. The lead angle is then γ such that

$$\tan \gamma = \frac{l}{2\pi r}. \quad (13)$$

We can use the time interpretation of t to find a formula for moving back and forth between the v and γ representations. If equation (12) holds, then it takes 2π seconds for a point on the helix to describe one complete turn. In this amount of time the point moves a distance $l = 2\pi v$ along the axis of the helix, which corresponds to the lead. From equation (13) we obtain

$$\tan \gamma = \frac{v}{r}. \quad (14)$$

[†]Notice that this unit vector is not properly defined if the tangent is constant along the curve, i.e., in the degenerate case of a straight cable. If a straight cable is to be modelled, a valid system can be constructed by rotating the original Cartesian system such that $x = x_1$ aligns with the cable. To treat cases in which a cable curves along some segments but is straight along others, algorithms should monitor $|\mathbf{n}(s')|$ as x is varied.

Therefore when we exhaust the usefulness of the time/speed parameterization of the helix we can view v instead as merely a constant involving the *real* parameters of the helix, γ and r :

$$v(\gamma) = r \tan \gamma. \quad (15)$$

For our purposes, the helix in equation (12) is a special case, in which the axis of the helix is straight and parallel to the x_1 coordinate axis. Our task is to relax these to allow for an axis that varies. The special helix equation can be re-written

$$\begin{aligned} \mathbf{f} = \begin{bmatrix} f_1(s') \\ f_2(s') \\ f_3(s') \end{bmatrix} &= \begin{bmatrix} s' \\ r \cos s'/v \\ r \sin s'/v \end{bmatrix} \\ &= \begin{bmatrix} s' \\ 0 \\ 0 \end{bmatrix} + \begin{bmatrix} 0 \\ r \cos s'/v \\ r \sin s'/v \end{bmatrix} = \mathbf{c} + \mathbf{h}. \end{aligned} \quad (16)$$

In the last expression, the vector position of a point along the helix is broken up into the sum of two vectors: first, a vector taking us from the origin to the projection of the point onto the axis of the helix; and second, a vector taking us from the axis of the helix to the perimeter (Figure 2).

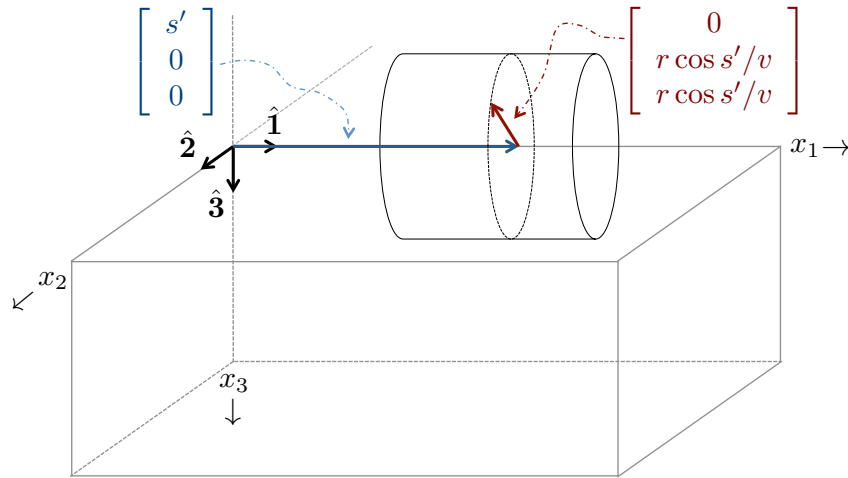


FIG. 2. A decomposition of the position vector of a point along a helix. A helix wound around the x_1 axis forms an envelope as illustrated; our decomposition involves the sum of two vectors, the first pointing from the origin to the projection of the desired point on the axis of the helix (blue), and the second, in the plane normal to the x_1 axis, pointing the rest of the way (red).

Equation (16) is in the form in which we wanted to describe the fibre, back when we wrote down equation (2). The only problem is that it is still good only for the special case of the straight helix. Let us next extend the last line of equation (16) to accommodate the general case, as illustrated in Figure 3. We start by writing down equation (2) again:

$$\begin{bmatrix} f_1(s') \\ f_2(s') \\ f_3(s') \end{bmatrix} = \begin{bmatrix} c_1(s') \\ c_2(s') \\ c_3(s') \end{bmatrix} + \begin{bmatrix} h_1(s') \\ h_2(s') \\ h_3(s') \end{bmatrix}. \quad (17)$$

To describe a point along the fibre, we must provide the two terms on the right hand side of this expression. Equations (6)-(7) from the previous section provide the first term, namely, the position vector of any point along the axis of the deviated cable and the arc-length to that point from $x = x_1 = 0$. This is represented by the grey dashed line in Figure 3a.

In the varying coordinate system derived in the previous section, namely $\{\hat{\mathbf{t}}(s'), \hat{\mathbf{n}}(s'), \hat{\mathbf{b}}(s')\}$, we always rotate ourselves so that the second term in the general case in equation (17) still looks exactly like the second term in equation (12):

$$\begin{bmatrix} 0 \\ r \cos s'/v \\ r \sin s'/v \end{bmatrix}. \quad (18)$$

The only remaining task is, therefore, for each position s' , to transform equation (18) into the original Cartesian system in which the terms of equation (17) are written. We do this by operating on it with the rotation matrix designed to take us from the $\{\hat{\mathbf{t}}, \hat{\mathbf{n}}, \hat{\mathbf{b}}\}$ system to the $\{\hat{\mathbf{1}}, \hat{\mathbf{2}}, \hat{\mathbf{3}}\}$ system. Then we add the two vector components together obtaining $\mathbf{f} = \mathbf{c} + \mathbf{h}$, that is,

$$\begin{bmatrix} f_1(s') \\ f_2(s') \\ f_3(s') \end{bmatrix} = \begin{bmatrix} c_1(s') \\ c_2(s') \\ c_3(s') \end{bmatrix} + \begin{bmatrix} \hat{\mathbf{1}} \cdot \hat{\mathbf{t}}(s') & \hat{\mathbf{1}} \cdot \hat{\mathbf{n}}(s') & \hat{\mathbf{1}} \cdot \hat{\mathbf{b}}(s') \\ \hat{\mathbf{2}} \cdot \hat{\mathbf{t}}(s') & \hat{\mathbf{2}} \cdot \hat{\mathbf{n}}(s') & \hat{\mathbf{2}} \cdot \hat{\mathbf{b}}(s') \\ \hat{\mathbf{3}} \cdot \hat{\mathbf{t}}(s') & \hat{\mathbf{3}} \cdot \hat{\mathbf{n}}(s') & \hat{\mathbf{3}} \cdot \hat{\mathbf{b}}(s') \end{bmatrix} \begin{bmatrix} 0 \\ r \cos s'/v(\gamma) \\ r \sin s'/v(\gamma) \end{bmatrix}. \quad (19)$$

2b. Arc-length s along the fibre

The arc-length s' it should be re-emphasized is not the arc-length around the helix, but the arc-length of the cable axis about which the helix winds. The arc-length along the helix, s , is related to s' by

$$s = \left[1 + \frac{r^2}{v^2}\right]^{1/2} \times s' = \left[1 + \frac{1}{\tan^2 \gamma}\right]^{1/2} \times s'. \quad (20)$$

This arc-length measure is critical to the model because this is the physical dimension along which fibre measurements are made. That is, when a certain strain is observed by the fibre interrogator, the interrogator returns the location of this strain in units of distance s .

2c. Fibre tangents

The various quantities needed to track (1) all positions along the deviated cable and its helical-wound fibre, and (2) the tangent direction to the fibre at each of these positions, are summarized as follows. If the axis of a cable around which a helical fibre is wound is described in some suitable reference Cartesian system by $[c_1, c_2, c_3]^T$, with s' representing the arc-length of the cable axis, then a point on the helical fibre at a distance s' along this axis has the position vector $\mathbf{f} = [f_1(s'), f_2(s'), f_3(s')]^T$, where

$$\begin{bmatrix} f_1(s') \\ f_2(s') \\ f_3(s') \end{bmatrix} = \begin{bmatrix} c_1(s') \\ c_2(s') \\ c_3(s') \end{bmatrix} + \begin{bmatrix} \hat{\mathbf{1}} \cdot \hat{\mathbf{t}}(s') & \hat{\mathbf{1}} \cdot \hat{\mathbf{n}}(s') & \hat{\mathbf{1}} \cdot \hat{\mathbf{b}}(s') \\ \hat{\mathbf{2}} \cdot \hat{\mathbf{t}}(s') & \hat{\mathbf{2}} \cdot \hat{\mathbf{n}}(s') & \hat{\mathbf{2}} \cdot \hat{\mathbf{b}}(s') \\ \hat{\mathbf{3}} \cdot \hat{\mathbf{t}}(s') & \hat{\mathbf{3}} \cdot \hat{\mathbf{n}}(s') & \hat{\mathbf{3}} \cdot \hat{\mathbf{b}}(s') \end{bmatrix} \begin{bmatrix} 0 \\ r \cos s'/v(\gamma) \\ r \sin s'/v(\gamma) \end{bmatrix}. \quad (21)$$

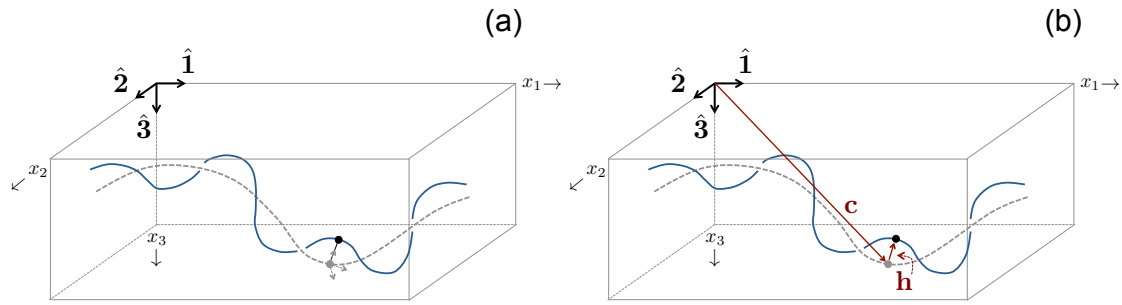


FIG. 3. Describing a helix winding around an arbitrarily curved cable. (a) The problem is a generalization of the problem of describing a helix winding around one coordinate axis. (b) The position of a point on the fibre is decomposed into two contributing vectors, one, a vector to the point on the axis of the cable closest to the point along the fibre to be described, and two, a vector from the axis to the desired point on the fibre. The latter is in the plane perpendicular to the tangent vector at the former.

Several re-parameterizations of this formula are also convenient to develop. To re-express $f(s')$ as instead $f(s)$, i.e., in terms of total arc-length s rather than axial arc-length s' the change of variables

$$s'(s) = \left[1 + \frac{r^2}{v^2} \right]^{1/2} s, \tag{22}$$

following from equation (20), can be used.

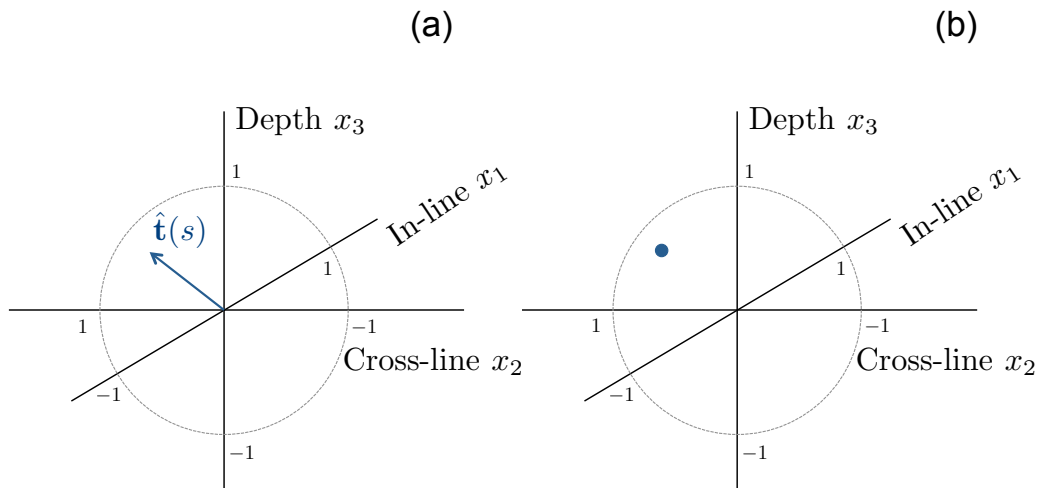


FIG. 4. Each point along fibre is considered to be at the centre of a small interval over which the fibre “senses” one tangent direction. The set of tangent directions occurring along a given fibre or fibre segment can be visualized by drawing a unit vector parallel to the tangent direction (a), or simply plotting a dot on the transparent unit ball of all such unit vectors (b).

The second cable parameterization in equation (6), in which the 2 and 3 components of position are given in terms of the first component of position x , can also be enacted, this time by making the change of variables $x = f_1$ and $s = s(x)$ within equations (21)–(22),

where

$$s(x) = \int_0^x dx' \left[1 + \left(\frac{df_2}{dx'} \right)^2 + \left(\frac{df_3}{dx'} \right)^2 \right]^{1/2}. \quad (23)$$

Finally, in the $f(s)$ parameterization, the tangent

$$\hat{\mathbf{t}}(s) = \frac{d\mathbf{f}}{ds}, \quad (24)$$

can be calculated. This quantity $\hat{\mathbf{t}}(s)$ in particular will be important to store, as it will be the projection of seismic strain on this direction which produces a DAS signal in our model.

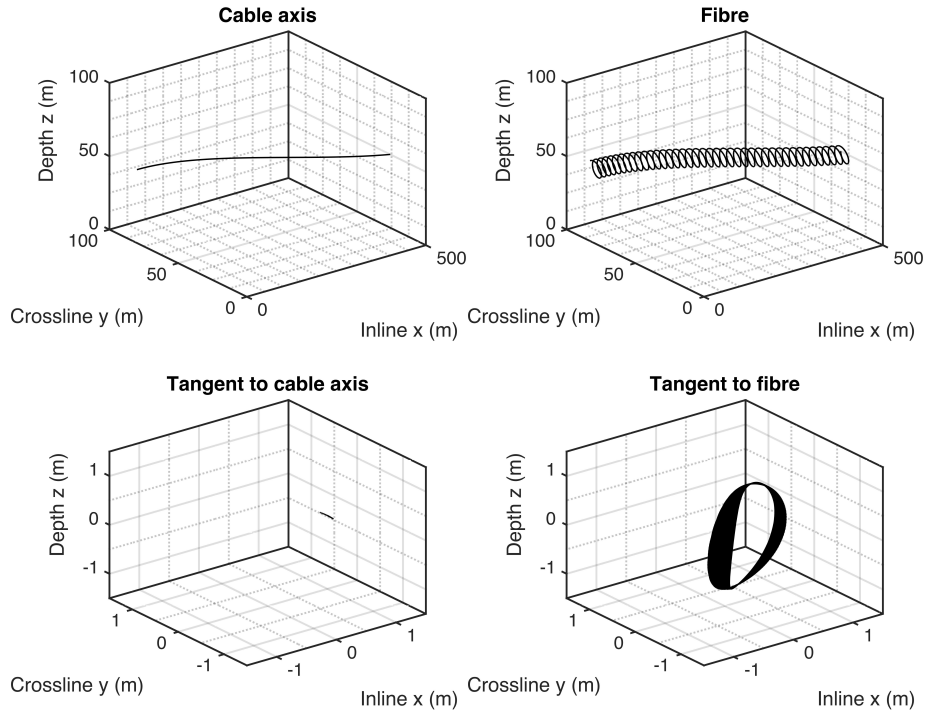


FIG. 5. Top left: cable axis; top right: fibre; bottom left: tangents explored by the cable axis; bottom right: tangents explored by the fibre.

It will be useful, when applying these results to the response of a DAS fibre system, to be able to characterize the range of different tangent directions generated by a particular deviated cable containing a helical-wound fibre. Each point along the fibre generates a single unit tangent vector $\hat{\mathbf{t}}(s)$, which in turn can be represented as a point on a unit sphere centred on the origin in (x_1, x_2, x_3) ; the point the tangent vector touches (see Figure 4). Therefore, as we traverse the fibre, unit tangent vectors will be continuously generated, some new, and some having already been generated at earlier points along the fibre, curves and/or areas on the surface of the unit sphere will be drawn and/or filled in. A regular and periodic cable/fibre system will tend to generate a Lissajous figure on this sphere.

Let us put all of these elements together with two examples. In Figure 5, four panels illustrate an example fibre geometry. In the top left panel a cable is buried at a fixed depth

with a low degree of curvature along its lateral extent. In the top right panel a helix (unrealistically large for illustration purposes) is wound around this curve (parameters $r = 4\text{m}$, $v = 2\text{m/s}$). The bottom left and right panels illustrate the tangents explored by each of these curves (the left being the set of tangents a straight fibre in the same cable would experience). Without the helix, we find a paucity of tangent directions, but with the helix a “strip” of tangents is seen.

In Figure 6 a slightly more complicated example is provided, in which the cable itself winds in a helix (with a radius of 30m and a speed of 8m/s , i.e., with a cable winding rate of 0.125 cycles/m along the x_1 axis), and so we have a fibre wound in a helix ($r=4\text{m}$, $v=2\text{m/s}$) around a cable which is also a helix, producing a “twisted telephone cord” shape. In the lower panels, we observe that the tangents produced by a lone helix (such as the cable axis) describe a circle on the unit sphere; whereas, the tangents experienced by the fibre are much more widespread, and one begins to see a larger fraction of the surface of the unit sphere being traced out.

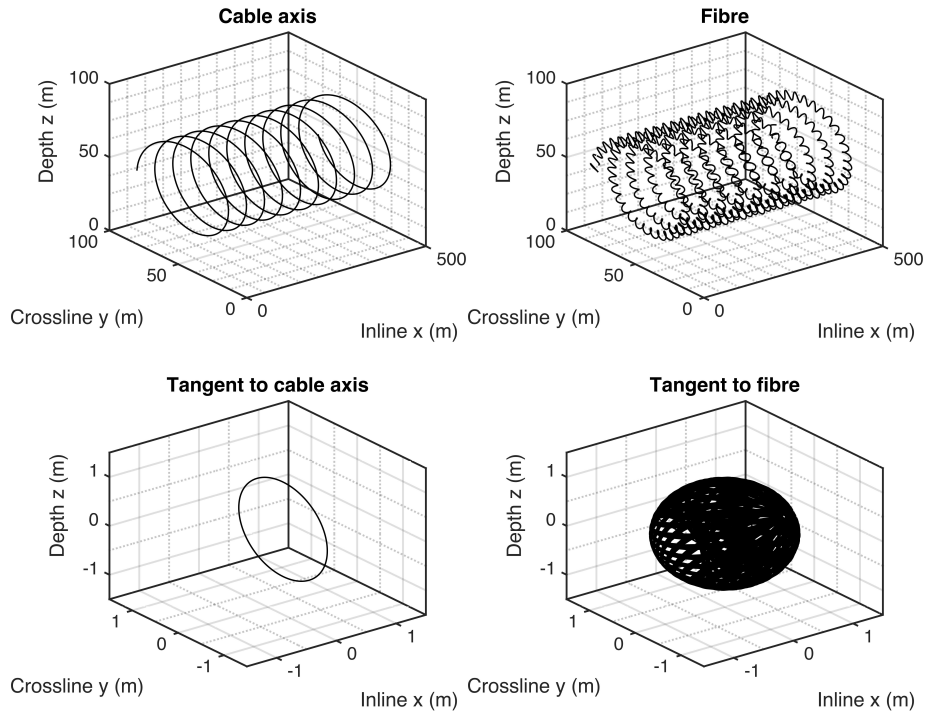


FIG. 6. Top left: cable axis; top right: fibre; bottom left: tangents explored by the cable axis; bottom right: tangents explored by the fibre.

3. Gauge length

The instantaneous strain at a position s along a DAS fibre is proportional to the count of photons returning along the fibre at time $\tau = 2s/c_f$, where c_f is the axial velocity of light in the fibre. Since photons are *counted* to determine the strain, and it takes time to count, it follows that the time τ should actually be interpreted as the midpoint of an integration interval $(\tau - \Delta\tau/2, \tau + \Delta\tau/2)$, with $\Delta\tau$ being as small as possible while maintaining

the desired SNR. It further follows that a DAS fibre response has a characteristic spatial interval $(s - \Delta s/2, s + \Delta s/2)$, where $\Delta s = (c_f/2)\Delta\tau$, to which we assign a single strain value. This practical limit on DAS spatial resolution is the *gauge length*.

In the current geometrical model a chosen gauge length Δs is imposed onto the existing fibre geometry, i.e., the quantities calculated so far. An ‘impose gauge length’ function can be called, the output of which is a new full set of the geometrical position and arc-length quantities, averaged over the selected gauge length. These new vector quantities can be re-submitted to the functions computing tangents etc., and a full set of newly-resampled geometrical fibre/cable outputs created.

APPLICATIONS

The purpose of the model described in the previous section is to provide an all-purpose tool for analysis and appraisal of a planned or existing fibre, and is particularly designed to do so when the fibre has an interesting or unusual geometry (with or without a helical wind). In this section we explore four of the possible uses of the model.

I. Embedding fibre in a snapshot of an elastic field

Once a fibre has been given a geometrical form and all auxiliary quantities have been calculated, it may be embedded into a snapshot of an elastic wave field and its response to that wave field computed. The current version of the model accepts either (1) a vector displacement as input, returning as output the component of displacement tangent to the fibre at all points along its arc-length, or (2) a tensor strain as input, returning as output the component of normal strain in the direction tangent to the fibre at all points along its arc-length.

The arc-length (and other) vectors describing the fibre are discretized with sampling Δs of a certain size, and the snapshot of the field is assumed to be discretized with a different sampling interval. The fibre is overlain on the cells of the snapshot of the field and discrete points on the fibre are associated with cells in the field as per Figure 7.

To exemplify the procedure, we generate a 3D constant elastic wave field with uniform displacement pointing in the $y = x_2$, or crossline, direction. A “helix on a helix” fibre geometry is embedded in the volume containing the field. The fibre is depicted in Figure 8, with the right panel illustrating the helical cable and the left panel illustrating the helix winding around the cable (with nonphysically large radius).

In Figure 9 the characteristic sampling of a constant vector wave field by a helix-on-helix fibre appears, as a signal varying with two frequencies, one for each “level” of helix.

The effect of increasing the gauge length of the fibre can be analyzed in this context also. In Figure 10 a 2m gauge length is imposed on the same fibre, and the difference between what a “perfect” fibre sees (top panel) and what this more realistic fibre sees (middle panel) can be clearly discerned.

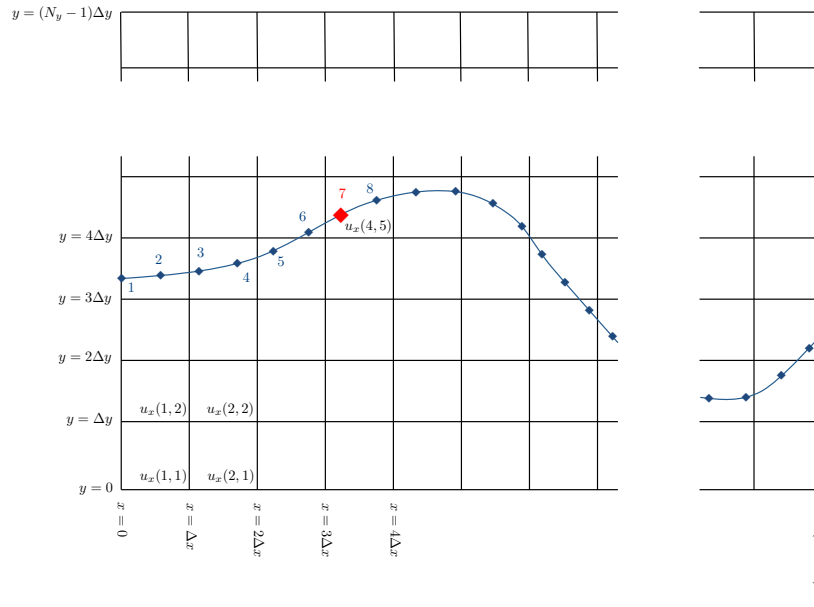


FIG. 7. Fibre to wave field snapshot discretization and binning scheme. The (e.g.) 7th element of any vector representing variation along the arc-length of the fibre senses the (4, 5)th element of the x -component of displacement.

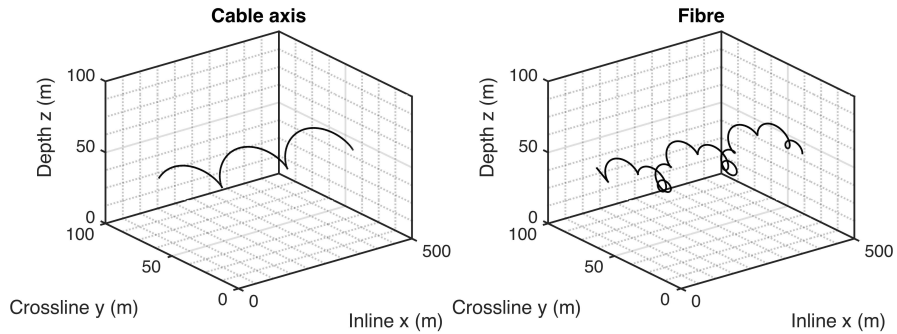


FIG. 8. Cable (left) and fibre (right) used to test vector wave field sampling.

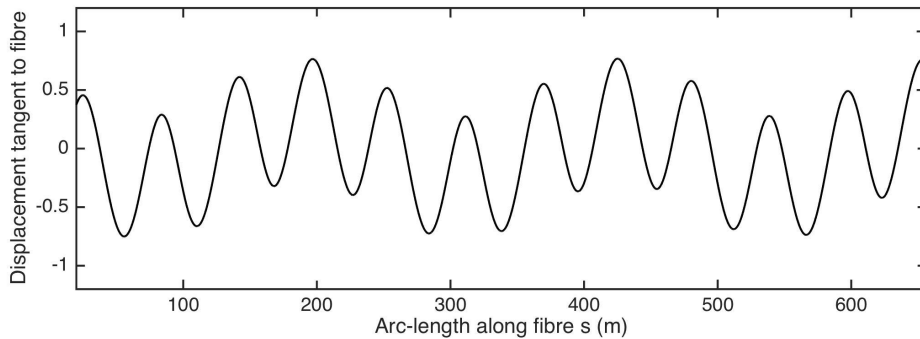


FIG. 9. The displacement sensed by the two-helix fibre along its arc-length.

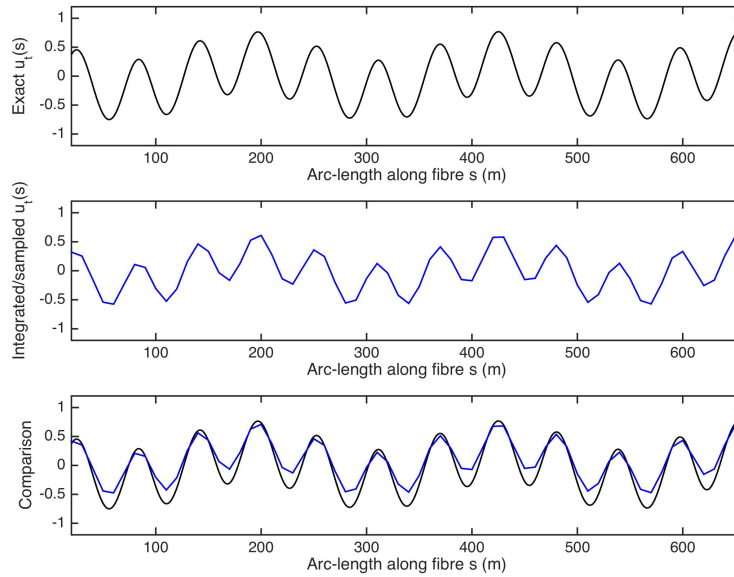


FIG. 10. Top panel: fibre response absent a gauge length (i.e., the ideal case); middle panel: fibre response with a 2m gauge length; bottom panel: comparison.

II. Reconstruction of vector displacement

A simple inverse problem for the determination of the vector displacement in the vicinity of the fibre, given as input measurements of the tangential displacement over a range of fibre intervals can be set up. The key assumption made here is that the strain along an interval of fibre can be processed to approximate the component of displacement in the direction tangent to the fibre at that interval. The vector displacement cannot be determined over arbitrarily short intervals of the fibre, however, but rather must be estimated within some finite reconstruction window (see Figure 11). If a window can be chosen to be (1) large enough to contain the range of fibre tangent directions necessary to constrain three components of displacement, and simultaneously (2) small enough that within it the wave field is nearly constant, the estimation is well posed.

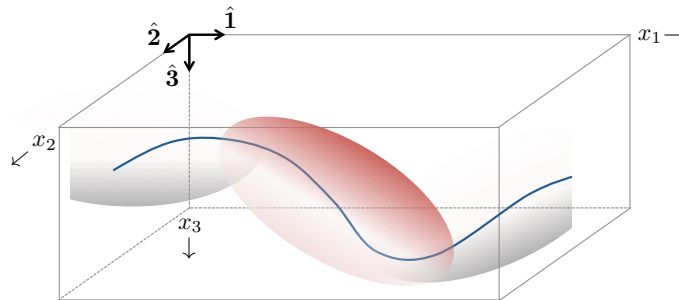


FIG. 11. A key aspect of the vector and/or tensor reconstruction is that it must occur within a reconstruction window within which the field must be close to constant.

The inverse problem is set up from the rotation matrices necessary to transform a vector from the experimental coordinate system $(\hat{\mathbf{1}}, \hat{\mathbf{2}}, \hat{\mathbf{3}})$ to the coordinate system based on the

tangent at the current value of arc-length along the fibre s , which are of the form

$$\begin{bmatrix} u_t \\ u_n \\ u_b \end{bmatrix} = \begin{bmatrix} \hat{\mathbf{t}} \cdot \hat{\mathbf{1}} & \hat{\mathbf{t}} \cdot \hat{\mathbf{2}} & \hat{\mathbf{t}} \cdot \hat{\mathbf{3}} \\ \hat{\mathbf{n}} \cdot \hat{\mathbf{1}} & \hat{\mathbf{n}} \cdot \hat{\mathbf{2}} & \hat{\mathbf{n}} \cdot \hat{\mathbf{3}} \\ \hat{\mathbf{b}} \cdot \hat{\mathbf{1}} & \hat{\mathbf{b}} \cdot \hat{\mathbf{2}} & \hat{\mathbf{b}} \cdot \hat{\mathbf{3}} \end{bmatrix} \begin{bmatrix} u_1 \\ u_2 \\ u_3 \end{bmatrix}. \quad (25)$$

Notice that the first inner product in this system (top row by single column) generates the tangential displacement u_t for the particular tangent direction $\hat{\mathbf{t}}$ under consideration. Assuming access to N such tangents (coming from N positions on the fibre, labelled by their arc-length locations s_1, s_2, \dots, s_N), a new matrix equation, built up of repeated instances of the topmost inner product in equation (25) can be constructed:

$$\begin{bmatrix} u_t(s_1) \\ u_t(s_2) \\ \vdots \\ u_t(s_N) \end{bmatrix} = \begin{bmatrix} \hat{\mathbf{t}}(s_1) \cdot \hat{\mathbf{1}} & \hat{\mathbf{t}}(s_1) \cdot \hat{\mathbf{2}} & \hat{\mathbf{t}}(s_1) \cdot \hat{\mathbf{3}} \\ \hat{\mathbf{t}}(s_2) \cdot \hat{\mathbf{1}} & \hat{\mathbf{t}}(s_2) \cdot \hat{\mathbf{2}} & \hat{\mathbf{t}}(s_2) \cdot \hat{\mathbf{3}} \\ \vdots & \vdots & \vdots \\ \hat{\mathbf{t}}(s_N) \cdot \hat{\mathbf{1}} & \hat{\mathbf{t}}(s_N) \cdot \hat{\mathbf{2}} & \hat{\mathbf{t}}(s_N) \cdot \hat{\mathbf{3}} \end{bmatrix} \begin{bmatrix} u_1 \\ u_2 \\ u_3 \end{bmatrix}. \quad (26)$$

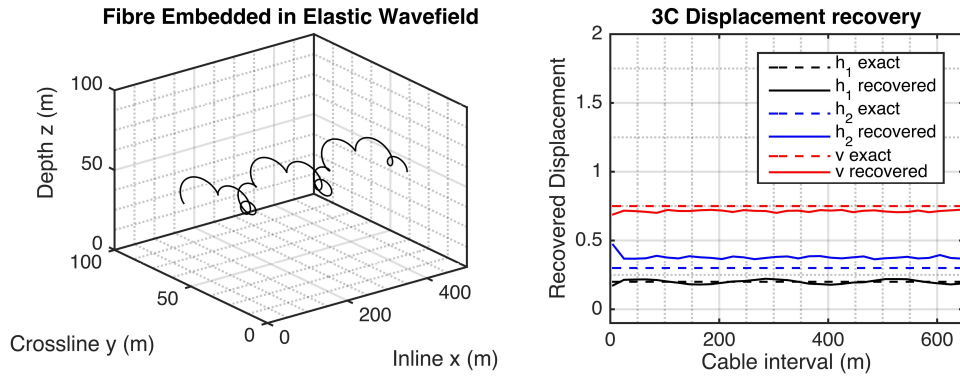


FIG. 12. An example with a relatively broad exploration of tangent directions. Left: fibre embedded in a constant vector wave field ($u_x = 0.2, u_y = 0.3, u_z = 0.75$). Right: recovered signals (solid) versus exact signals (dashed).

This is the forward problem: given a constant vector field $[u_1, u_2, u_3]^T$, equation (26) returns the projection of this vector into each tangent direction. Re-writing the equation as

$$\begin{bmatrix} u_t(s_1) \\ u_t(s_2) \\ \vdots \\ u_t(s_N) \end{bmatrix} = \mathbf{P} \begin{bmatrix} u_1 \\ u_2 \\ u_3 \end{bmatrix}, \quad (27)$$

where

$$\mathbf{P} = \begin{bmatrix} \hat{\mathbf{t}}(s_1) \cdot \hat{\mathbf{1}} & \hat{\mathbf{t}}(s_1) \cdot \hat{\mathbf{2}} & \hat{\mathbf{t}}(s_1) \cdot \hat{\mathbf{3}} \\ \hat{\mathbf{t}}(s_2) \cdot \hat{\mathbf{1}} & \hat{\mathbf{t}}(s_2) \cdot \hat{\mathbf{2}} & \hat{\mathbf{t}}(s_2) \cdot \hat{\mathbf{3}} \\ \vdots & \vdots & \vdots \\ \hat{\mathbf{t}}(s_N) \cdot \hat{\mathbf{1}} & \hat{\mathbf{t}}(s_N) \cdot \hat{\mathbf{2}} & \hat{\mathbf{t}}(s_N) \cdot \hat{\mathbf{3}} \end{bmatrix}, \quad (28)$$

the inverse problem can be posed in (for instance) damped least-squares form:

$$\begin{bmatrix} u_1 \\ u_2 \\ u_3 \end{bmatrix}_{\text{dlsq}} = (\mathbf{P}^T \mathbf{P} + \alpha \mathbf{I})^{-1} \mathbf{P}^T \begin{bmatrix} u_t(s_1) \\ u_t(s_2) \\ \vdots \\ u_t(s_N) \end{bmatrix}. \quad (29)$$

An attractive feature of such a small estimation procedure is that we may consider one element of the reconstructed vector to have been (or to be likely to be) better or worse constrained than another, by dint of our earlier analysis of tangents and whether they spanned sufficient directions.

Returning to one of our original examples, let us try to reconstruct the fixed constant elastic displacement field we already analyzed. In Figure 12 we embed the fibre illustrated in the left panel into a constant elastic field, such that all of its windings can be used to estimate the elastic field. On the right panel the three components as computed over reconstruction windows chosen to be 10m, or, $5 \times$ the gauge length. On the left panel the recovered components are plotted individually in comparison with the exact answers. (Note: inline = h_1 , crossline = h_2 , depth = v .)

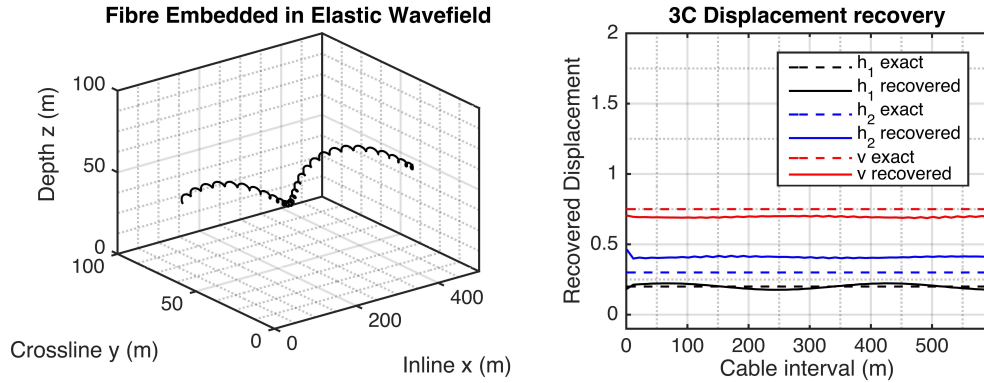


FIG. 13. An example with a relatively narrow exploration of tangent directions. Left: fibre embedded in a constant vector wave field ($u_x = 0.2, u_y = 0.3, u_z = 0.75$). Right: recovered signals (solid) versus exact signals (dashed).

III. Reconstruction of tensor strain

The same essential mathematical process of sequential projection onto the fibre tangent directions can also form the basis for an estimation problem for the tensor strain, once again provided a reconstruction window can be found which is large enough for many tangents to be contained within it and yet small enough that the strain is close to constant within it. The strain transforms as a tensor (in contrast to the displacement which transforms as a vector), and so the equation we start with has to be slightly more complex:

$$\begin{bmatrix} e_{tt} & e_{tn} & e_{tb} \\ e_{nt} & e_{nn} & e_{nb} \\ e_{bt} & e_{bn} & e_{bb} \end{bmatrix} = \begin{bmatrix} \hat{\mathbf{t}} \cdot \hat{\mathbf{1}} & \hat{\mathbf{t}} \cdot \hat{\mathbf{2}} & \hat{\mathbf{t}} \cdot \hat{\mathbf{3}} \\ \hat{\mathbf{n}} \cdot \hat{\mathbf{1}} & \hat{\mathbf{n}} \cdot \hat{\mathbf{2}} & \hat{\mathbf{n}} \cdot \hat{\mathbf{3}} \\ \hat{\mathbf{b}} \cdot \hat{\mathbf{1}} & \hat{\mathbf{b}} \cdot \hat{\mathbf{2}} & \hat{\mathbf{b}} \cdot \hat{\mathbf{3}} \end{bmatrix} \begin{bmatrix} e_{11} & e_{12} & e_{13} \\ e_{21} & e_{22} & e_{23} \\ e_{31} & e_{32} & e_{33} \end{bmatrix} \begin{bmatrix} \hat{\mathbf{t}} \cdot \hat{\mathbf{1}} & \hat{\mathbf{t}} \cdot \hat{\mathbf{2}} & \hat{\mathbf{t}} \cdot \hat{\mathbf{3}} \\ \hat{\mathbf{n}} \cdot \hat{\mathbf{1}} & \hat{\mathbf{n}} \cdot \hat{\mathbf{2}} & \hat{\mathbf{n}} \cdot \hat{\mathbf{3}} \\ \hat{\mathbf{b}} \cdot \hat{\mathbf{1}} & \hat{\mathbf{b}} \cdot \hat{\mathbf{2}} & \hat{\mathbf{b}} \cdot \hat{\mathbf{3}} \end{bmatrix}^{-1}.$$

The fibre senses e_{tt} in its own coordinate system. (1) Evaluating this matrix multiplication and extracting the explicit equation for e_{tt} , and (2) collecting these equations for all available tangential strains at fibre positions s_1, s_2, \dots, s_N , we form

$$\begin{bmatrix} e_{tt}(s_1) \\ e_{tt}(s_2) \\ \vdots \\ e_{tt}(s_N) \end{bmatrix} = \begin{bmatrix} \lambda_{11}^1 & \lambda_{12}^1 & \lambda_{13}^1 & \lambda_{21}^1 & \lambda_{22}^1 & \lambda_{23}^1 & \lambda_{31}^1 & \lambda_{32}^1 & \lambda_{33}^1 \\ \lambda_{11}^2 & \lambda_{12}^2 & \lambda_{13}^2 & \lambda_{21}^2 & \lambda_{22}^2 & \lambda_{23}^2 & \lambda_{31}^2 & \lambda_{32}^2 & \lambda_{33}^2 \\ \vdots & \vdots \\ \lambda_{11}^N & \lambda_{12}^N & \lambda_{13}^N & \lambda_{21}^N & \lambda_{22}^N & \lambda_{23}^N & \lambda_{31}^N & \lambda_{32}^N & \lambda_{33}^N \end{bmatrix} \begin{bmatrix} e_{11} \\ e_{12} \\ e_{13} \\ e_{21} \\ e_{22} \\ e_{23} \\ e_{31} \\ e_{32} \\ e_{33} \end{bmatrix},$$

where

$$\lambda_{ij}^k = \left(\hat{\mathbf{t}}(s_k) \cdot \hat{\mathbf{i}} \right) \left(\hat{\mathbf{t}}(s_k) \cdot \hat{\mathbf{j}} \right). \quad (30)$$

This again acting as the forward problem: in which the elements of a given strain tensor are projected onto the normal strain along the fibre element. Letting the matrix be \mathbf{L} , where

$$\mathbf{L} = \begin{bmatrix} \lambda_{11}^1 & \lambda_{12}^1 & \lambda_{13}^1 & \lambda_{21}^1 & \lambda_{22}^1 & \lambda_{23}^1 & \lambda_{31}^1 & \lambda_{32}^1 & \lambda_{33}^1 \\ \lambda_{11}^2 & \lambda_{12}^2 & \lambda_{13}^2 & \lambda_{21}^2 & \lambda_{22}^2 & \lambda_{23}^2 & \lambda_{31}^2 & \lambda_{32}^2 & \lambda_{33}^2 \\ \vdots & \vdots \\ \lambda_{11}^N & \lambda_{12}^N & \lambda_{13}^N & \lambda_{21}^N & \lambda_{22}^N & \lambda_{23}^N & \lambda_{31}^N & \lambda_{32}^N & \lambda_{33}^N \end{bmatrix},$$

a damped least-squares inversion takes the form:

$$\begin{bmatrix} e_{11} \\ e_{12} \\ e_{13} \\ e_{21} \\ e_{22} \\ e_{23} \\ e_{31} \\ e_{32} \\ e_{33} \end{bmatrix}_{\text{dlsq}} \approx (\mathbf{L}^T \mathbf{L} + \alpha \mathbf{I})^{-1} \mathbf{L}^T \begin{bmatrix} e_{tt}(s_1) \\ e_{tt}(s_2) \\ \vdots \\ e_{tt}(s_N) \end{bmatrix}. \quad (31)$$

In equation (31) the symmetry of the strain tensor has not been incorporated in the inversion – the data are being relied upon to find a value for e_{12} for instance which is equal to e_{21} . There would appear to be a few possibilities. First, leave it this way, and use the proximity of each strain element to its counterpart as an indicator of how well constrained the tensor strain is by the fibre response. Or, second, remove e_{21} , e_{31} and e_{32} from the model vector along with the corresponding columns from \mathbf{L} , and solve an inverse problem with 6 rather than 9 unknowns. Or, third, since the e_{31} column could potentially contain more useful information than the e_{13} column, and it may be difficult for a complex fibre to know if this is so, the problem could be left with 9 unknowns but, but solved with a model regularization term, which penalize $\|e_{13} - e_{31}\|$ and other symmetry pairs.

IV. Generalized $\cos \theta$ directionality rule for P-wave displacement

Suppose a P-wave were to be excited at a source point which is separated from a particular spot a distance s on a straight segment of fibre by the vector $\mathbf{r}(s)$. The P-wave particle displacement \mathbf{u} at the fibre is parallel to $\hat{\mathbf{r}}(s)$. If this direction of particle motion forms an angle θ with the direction of the fibre $\hat{\mathbf{t}}$, as illustrated in Figure 14, and the response of the fibre is *geophone-like*, namely the sensitivity is to the component of displacement parallel to $\hat{\mathbf{t}}$, the directionality for the fibre response (say, χ) will have a $\chi = \hat{\mathbf{t}} \cdot \hat{\mathbf{r}}(s) = \cos \theta$ character. The broadside ($\theta = 90^\circ$) response is therefore zero.

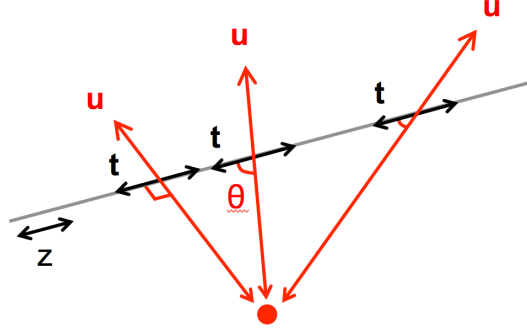


FIG. 14. Source / straight fibre configuration.

If the fibre is arbitrarily curved, but we have access to (1) the tangent at all points along its length, $\hat{\mathbf{t}}(s)$, and (2) the spatial coordinates in the experimental $(\hat{\mathbf{1}}, \hat{\mathbf{2}}, \hat{\mathbf{3}})$ system of each point s along its length, which are both provided by the model, the more complex $\hat{\mathbf{r}}(s)$ can be computed, and the directionality response is straightforwardly generalized to

$$\chi = \hat{\mathbf{t}}(s) \cdot \hat{\mathbf{r}}(s) = \cos \theta(s). \quad (32)$$

When plotted, therefore, the presence of the curved fibre will tend to produce either (a) the standard $\cos \theta$ curve, *provided* the horizontal axis is a generalized angle $\theta = \theta(s)$ calculated taking into account the co-varying fibre and radial unit vectors, or (b) a more complex function of s .

V. Generalized $\cos^2 \theta$ directionality rule for P-wave strain

Similar considerations can be used to generalize and characterize the strain directionality and consequent broadside insensitivity. That we can easily characterize the strain directionality for a P-wave derives from the fact that for a plane P-wave only one element of the strain tensor is nonzero: the normal strain in the direction parallel to propagation (i.e., the direction $\hat{\mathbf{r}}$ used in the previous section).

Suppose we focus on a point at arc-length s along the fibre, and at this point we wish to discuss the strain tensor in the native coordinate system (i.e., $\hat{\mathbf{t}}(s)$, $\hat{\mathbf{n}}(s)$, $\hat{\mathbf{b}}(s)$). The strain carried by the P-wave is naturally described in a system containing the propagation direction $\hat{\mathbf{r}}$, which we will label $\hat{\mathbf{r}}$, $\hat{\mathbf{2}}'$, $\hat{\mathbf{3}}'$, where the second two unit vectors span the plane perpendicular to the P-wave propagation direction. The strain tensor transforms from the

P-wave system to the local fibre system according to

$$\begin{bmatrix} e_{tt} & e_{tn} & e_{tb} \\ e_{nt} & e_{nn} & e_{nb} \\ e_{bt} & e_{bn} & e_{bb} \end{bmatrix} = \begin{bmatrix} \hat{\mathbf{t}} \cdot \hat{\mathbf{r}} & \hat{\mathbf{t}} \cdot \hat{\mathbf{2}}' & \hat{\mathbf{t}} \cdot \hat{\mathbf{3}}' \\ \hat{\mathbf{n}} \cdot \hat{\mathbf{r}} & \hat{\mathbf{n}} \cdot \hat{\mathbf{2}}' & \hat{\mathbf{n}} \cdot \hat{\mathbf{3}}' \\ \hat{\mathbf{b}} \cdot \hat{\mathbf{r}} & \hat{\mathbf{b}} \cdot \hat{\mathbf{2}}' & \hat{\mathbf{b}} \cdot \hat{\mathbf{3}}' \end{bmatrix} \begin{bmatrix} e_{rr} & e_{r2} & e_{r3} \\ e_{2r} & e_{22} & e_{23} \\ e_{3r} & e_{32} & e_{33} \end{bmatrix} \begin{bmatrix} \hat{\mathbf{t}} \cdot \hat{\mathbf{r}} & \hat{\mathbf{t}} \cdot \hat{\mathbf{2}}' & \hat{\mathbf{t}} \cdot \hat{\mathbf{3}}' \\ \hat{\mathbf{n}} \cdot \hat{\mathbf{r}} & \hat{\mathbf{n}} \cdot \hat{\mathbf{2}}' & \hat{\mathbf{n}} \cdot \hat{\mathbf{3}}' \\ \hat{\mathbf{b}} \cdot \hat{\mathbf{r}} & \hat{\mathbf{b}} \cdot \hat{\mathbf{2}}' & \hat{\mathbf{b}} \cdot \hat{\mathbf{3}}' \end{bmatrix}^{-1},$$

in general, but because we may set all but one of the strain components in the P-wave system to zero, we find that all but one of the transformed strain components are likewise zero:

$$\begin{bmatrix} e_{tt} & 0 & 0 \\ 0 & 0 & 0 \\ 0 & 0 & 0 \end{bmatrix} = \begin{bmatrix} \hat{\mathbf{t}} \cdot \hat{\mathbf{r}} & \hat{\mathbf{t}} \cdot \hat{\mathbf{2}}' & \hat{\mathbf{t}} \cdot \hat{\mathbf{3}}' \\ \hat{\mathbf{n}} \cdot \hat{\mathbf{r}} & \hat{\mathbf{n}} \cdot \hat{\mathbf{2}}' & \hat{\mathbf{n}} \cdot \hat{\mathbf{3}}' \\ \hat{\mathbf{b}} \cdot \hat{\mathbf{r}} & \hat{\mathbf{b}} \cdot \hat{\mathbf{2}}' & \hat{\mathbf{b}} \cdot \hat{\mathbf{3}}' \end{bmatrix} \begin{bmatrix} e_{rr} & 0 & 0 \\ 0 & 0 & 0 \\ 0 & 0 & 0 \end{bmatrix} \begin{bmatrix} \hat{\mathbf{t}} \cdot \hat{\mathbf{r}} & \hat{\mathbf{t}} \cdot \hat{\mathbf{2}}' & \hat{\mathbf{t}} \cdot \hat{\mathbf{3}}' \\ \hat{\mathbf{n}} \cdot \hat{\mathbf{r}} & \hat{\mathbf{n}} \cdot \hat{\mathbf{2}}' & \hat{\mathbf{n}} \cdot \hat{\mathbf{3}}' \\ \hat{\mathbf{b}} \cdot \hat{\mathbf{r}} & \hat{\mathbf{b}} \cdot \hat{\mathbf{2}}' & \hat{\mathbf{b}} \cdot \hat{\mathbf{3}}' \end{bmatrix}^{-1}.$$

So, expanding the matrix multiplication and focusing on the top left element, a simple transformation from the normal strain carried by the P-wave to the normal strain experienced by the fibre is

$$[\text{fibre strain}] = (\hat{\mathbf{t}}(s) \cdot \hat{\mathbf{r}}(s)) [\text{P-wave strain}] (\hat{\mathbf{t}}(s) \cdot \hat{\mathbf{r}}(s)). \quad (33)$$

Notice that if the fibre tangent were chosen to be constant and parallel to the depth z axis (as illustrated in Figure 14), and if θ is defined as the angle of incidence of the P-wave on the fibre, this directionality reduces to

$$[\text{vertical fibre strain}] = (\hat{\mathbf{z}} \cdot \hat{\mathbf{r}}) e_{rr} (\hat{\mathbf{z}} \cdot \hat{\mathbf{r}}) = [\text{P-wave strain}] \cos^2 \theta, \quad (34)$$

the standard result characterizing broadside insensitivity in walkaway VSP using fibre.

If the fibre has an arbitrarily curvature the strain carried by a P-wave thus projects onto the fibre in a more complex fashion. If the strain experience by the fibre is plotted as a function of arc-length, then when we move from a straight to a curved fibre that s dependence becomes increasingly complicated in response. If instead the projected strain is parameterized in terms of an s -dependent angle θ where

$$\theta(s) = \cos^{-1} (\hat{\mathbf{t}}(s) \cdot \hat{\mathbf{r}}(s)), \quad (35)$$

we expect to recover the same linear $[\text{strain}] \propto \cos^2 \theta$, with the added complexity of the geometry of the fibre absorbed in the nonlinear $\theta(s)$.

To confirm this within the geometrical model, a straight fibre is embedded in a 3D medium containing a P-wave source point as illustrated in Figure 15a. A constant displacement and/or strain carried by the P-wave with one nonzero component in the radial direction (between the source point and any point on the fibre under consideration) is projected onto the tangent direction of the fibre. In Figure 15b the strain and displacement so projected are plotted as a function of the incidence angle θ , and in Figure 15c the same quantities are plotted against arc-length s . These results match the broadside insensitivity results discussed in the literature (e.g., Mateeva et al., 2014). If the exercise is repeated with a two-level helical fibre (Figure 16a), and the results are plotted against the new $\theta(s)$

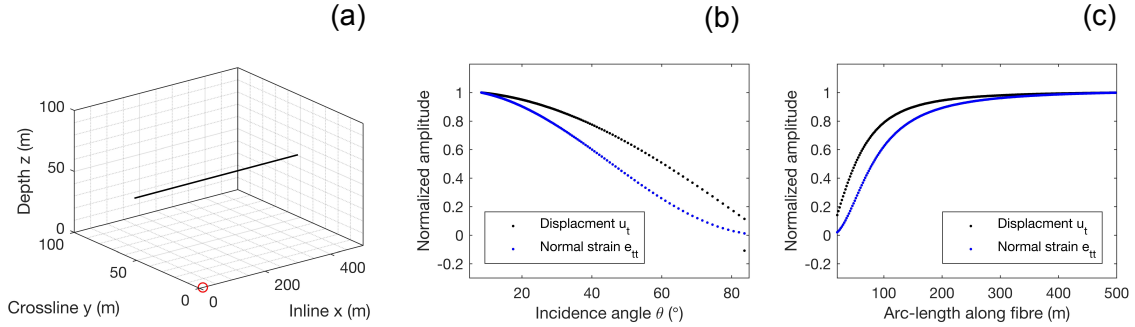


FIG. 15. (a) Straight fibre in the vicinity of a P-wave source point (red circle); (b) normalized strain (blue) and displacement (black) plotted versus angle of incidence θ ; (c) normalized strain (blue) and displacement (black) plotted versus arc-length s .

computed using equation (35), projected strain versus θ has exactly the same shape as it had in the case of the straight fibre (Figure 16b); however, closer comparison of Figures 15b and 16b reveals that the latter is now sampled irregularly in accordance with the more complex $\theta(s)$ relationship. The complexity of the altered fibre geometry is more clearly visible in the plot of strain and displacement versus arc-length s (Figure 16c).

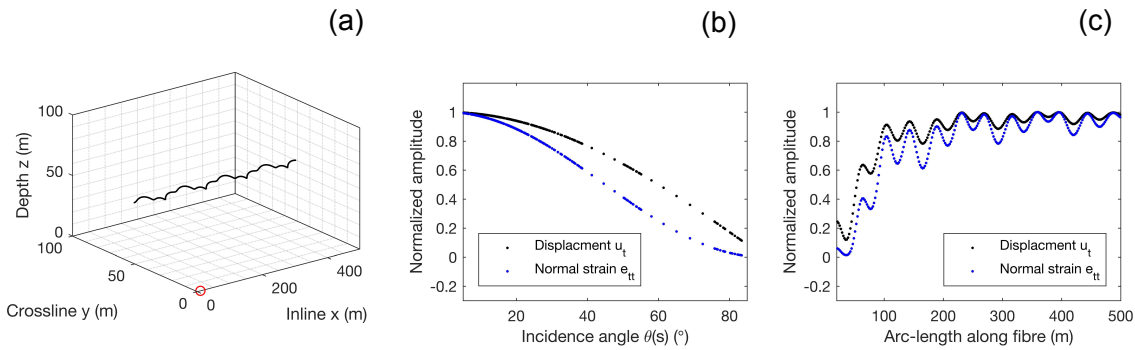


FIG. 16. (a) Straight fibre in the vicinity of a P-wave source point (red circle); (b) normalized strain (blue) and displacement (black) plotted versus angle of incidence θ ; (c) normalized strain (blue) and displacement (black) plotted versus arc-length s .

CONCLUSIONS

Some of the important issues facing DAS technology are geometrical in nature, principle of these being the broadside insensitivity issue, and the reconstruction of multicomponent displacement or strain quantities. These issues can be to a degree overcome by increasing the geometrical complexity of the fibre, thus increasing the variety of directions “explored” by its direction of sensitivity, the tangent direction. However, although introducing such curvature might enrich otherwise weak broadside response, it raises the challenge of understanding exactly what is being measured, a question which can only be adequately addressed by keeping a very careful account of all the geometrical features of the fibre. To do this we have assembled a fibre model which enumerates all positions and tangents of an arbitrarily complex fibre, and from this derives generalized directivity results as well as simple inverse procedures for the reconstruction of vector and tensor quantities

being carried by a seismic wave. The model is expected to be useful in both design of and characterization of experiments.

ACKNOWLEDGEMENTS

We thank the sponsors of CREWES for continued support. This work was funded by CREWES industrial sponsors and NSERC (Natural Science and Engineering Research Council of Canada) through the grant CRDPJ 461179-13.

REFERENCES

- Ajo-Franklin, J., Lindsey, N., Dou, S., Daley, T. M., Freifeld, B., Martin, E. R., Robertson, M., Ulrich, C., and Wagner, A., 2015, A field test of Distributed Acoustic Sensing for ambient noise recording: SEG Expanded Abstracts.
- Born, M., and Wolf, E., 1999, Principles of optics: Cambridge University Press, 7th edn.
- Chalenski, D., Tatanova, M., Du, Y., Lopez, J., Mateeva, A., and Potters, H., 2016, Climbing the staircase of ultra-low cost 4D monitoring of deepwater fields using DAS-VSP: SEG Expanded Abstracts.
- Daley, T. M., Freifeld, B. M., Ajo-Franklin, J., Dou, S., Pevzner, R., Shulakova, V., Kashikar, S., Miller, D. E., Goetz, J., Hennings, J., and Lueth, S., 2013, Field testing of fiber-optic distributed acoustic sensing (DAS) for subsurface seismic monitoring: *The Leading Edge*, **32**, No. 6.
- Kreyszig, E., 1991, Differential Geometry: Dover Publications, 1st edn.
- Kuvshinov, B. N., 2016, Interaction of helically wound fibre-optic cables with plane seismic waves: *Geophysical Prospecting*, **64**, 671–688.
- Mateeva, A., Lopez, J., Mestayer, J., Wills, P., Cox, B., Kiyashchenko, D., Yang, Z., Berlang, W., Detomo, R., and Grandi, S., 2013, Distributed Acoustic Sensing (DAS) for reservoir monitoring with VSP: *The Leading Edge*, **32**, 1278–1283.
- Mateeva, A., Lopez, J., Potters, H., Mestayer, J., Cox, B., Kiyashchenko, D., Wills, P., Grandi, S., Hornman, K., Kuvshinov, B., Berlang, W., Yang, Z., and Detomo, R., 2014, Distributed acoustic sensing for reservoir monitoring with vertical seismic profiling: *Geophysical Prospecting*, **62**, 679–692.
- Mateeva, A., Mestayer, J., Cox, B., Kiyashchenko, D., Wills, P., Lopez, J., Grandi, S., Hornman, K., Lumens, P., Franzen, A., Hill, D., and Roy, J., 2012, Advances in Distributed Acoustic Sensing (DAS) for VSP: SEG Expanded Abstracts.
- Mestayer, J., Cox, B., Wills, P., Kiyashchenko, D., Lopez, J., Costello, M., Bourne, S., Ugueto, G., Lupton, R., Solano, G., Hill, D., and Lewis, A., 2011, Field trials of distributed acoustic sensing for geophysical monitoring: SEG Expanded Abstracts.
- Parker, T., Shatalin, S., and Farhadiroushan, M., 2014, Distributed Acoustic Sensing - a new tool for seismic applications: *First Break*, **32**, 61–69.